Nov 13th, 12:00 AM

Geometric Nonlinear Dynamic Analysis of Locally Buckled Frames

George E. Blandford

Shien T. Wang

Neng T. Wang

Seventh International Specialty Conference on Cold-Formed Steel Structures
St. Louis, Missouri, U.S.A., November 13-14, 1984

GEOMETRIC NONLINEAR DYNAMIC ANALYSIS OF LOCALLY BUCKLED FRAMES

by

George E. Blandford[1], Shien T. Wang[2], and Neng T. Wang[3]

INTRODUCTION

The dynamic analysis of framework structural systems has been a subject of investigation due to the rapid development of high speed computers and matrix methods of structural analysis. However, the inclusion of beam-column and P-delta secondary moments and the influence of local buckling on the response of structural systems is lacking. Therefore, the influence of both secondary moments and reduced stiffness caused by local buckling on the dynamic response of framework structural systems requires investigation.

The purpose of this paper is to investigate both the static and dynamic response of structural frames in the post-local-buckling range including the influence of secondary moments. The effective width concept is used to represent the post-local-buckling strength in the compression plate elements of the frame members. Previous research on beams and columns (Refs. 3, 8 and 13) has shown that the effective width concept is valid for dynamic analysis. The inclusion of post-local-buckling behavior results in varying axial and flexural rigidities along the frame member lengths. Blandford, Wang and Wang (Ref. 2) used a finite element approximation to represent the stiffness distribution in the post-local-buckling range. Furthermore, they utilized a consistent mass approximation, neglected damping and implemented an incremental Wilson-θ formulation for the time integration of the nonlinear equations. The present investigation also used a consistent mass formulation and neglects the dampling. However, an exact elastic stiffness matrix is

[1] Assistant Professor and [2] Professor, Department of Civil Engineering, University of Kentucky, Lexington, KY 40506-0046; [3] Structural Engineer, Gannet-Fleming, Inc., Harrisburg, PA

presented to represent both the axial and flexural rigidities in the post-local-buckling range. First-order geometric nonlinearity (secondary moments) is approximated by using finite element interpolation. The solution of the resulting nonlinear equations is obtained by using a load correcting analysis procedure coupled with the implicit Wilson-θ time integration scheme (Ref. 12). The nonlinear solution algorithm and its performance for both static and dynamic problems are presented.

METHOD OF ANALYSIS

Postbuckling Strength of Locally Buckled Frames - The post-local-buckling strength is based on the effective width equation (Refs. 4, 9, and 10)

$$\frac{b}{t} = 0.95\sqrt{\frac{KE}{\sigma_{max}}}\left(1 - 0.95\xi\frac{t}{w}\sqrt{\frac{KE}{\sigma_{max}}}\right) \tag{1}$$

for

$$\frac{w}{t} \geq 0.64\sqrt{\frac{KE}{\sigma_{max}}} \tag{2}$$

in which b is the effective width of compression plate element, w is the flat width of the compression plate element, σ_{max} is the maximum edge stress, K is the coefficient determined by boundary conditions and aspect ratio for the compression plate element, and ξ is the modification factor based on experimental evidence and engineering judgement. For values of w/t smaller than $0.64\ EK/\sigma_{max}$, b = w. Equation 1 has been shown, through experimental verification, to be applicable to both stiffened and unstiffened plate elements if K is appropriately adjusted. The value of K can be evaluated by considering the relative dimensions of the section. For sections under uniform compression, K varies from 4.00 to 6.97 for stiffened plate elements and from 0.425 to 1.28 for unstiffened plate elements. For design considera-

tions, ξ may be taken as 0.22 and K may be taken as 0.50 and 4.0 for unstiffened and stiffened elements, respectively.

Consider the rigid plane frame shown in Fig. 1(a). The compression plate elements of the members in the frame will buckle locally and the neutral axis will shift away from the buckled compression plate element as shown in Fig. 1(c) if the compression elementstress is larger than the local buckling stress, σ_{cr}. The local buckling stress is derived from Eq. 2 by replacing σ_{max} with σ_{cr} and solving for σ_{cr}, i.e.,

$$\sigma_{cr} = 0.41\frac{KE}{(w/t)^2} \tag{3}$$

For the regions along the member length with compression elements stressed at levels larger than σ_{cr}, the reduced effective flexural rigidity $(EI)_{eff}$ and axial rigidity $(EA)_{eff}$ varies along the member length depending upon the stress magnitude. Consequently, in the post-local-buckling range the frame is composed of nonprismatic members as shown schematically in Fig. 1(d).

Dynamic Equilibrium - The dynamic equilibrium equations, neglecting damping forces, can be obtained from d'Alembert's principle as

$$\{F_I(t)\} + \{F_E(t)\} = \{P(t)\} \tag{4}$$

where $\{F_I(t)\}$, $\{F_E(t)\}$ and $\{P(t)\}$ are the inertial, elastic and external load vectors, respectively at time t. Evaluating Eq. 4 at time $t + \Delta t$, where Δt is the time increment, and writing the resulting equation in incremental form leads to

$$\{dF_I\} + \{dF_E\} = \{P(t+\Delta t)\} - \{F_I(t)\} - \{F_E(t)\} \tag{5a}$$

where d is used to signify the increment between time t and time $t + \Delta t$. Equation 5(a) can be rewritten in matrix form as

$$[M]\{d\ddot{v}\} + ([K_E(t)] + [K_G(t)])\{dv\}$$
$$= \{P(t+\Delta t)\} - \{F_I(t)\} - \{F_E(t)\} \quad (5b)$$

where [M] is the structure mass matrix (assumed linear), $[K_E(t)]$ is the structure tangent elastic stiffness matrix, $[K_G(t)]$ is the structure tangent geometric stiffness matrix, $\{d\ddot{v}\}$ is the incremental acceleration vector, $\{dv\}$ is the incremental displacement vector and the superposed dots signify order of time differentiation. Equation 5(b) is known as the load correcting incremental equilibrium equation due to the inclusion of the residual force imbalance in the current time step analysis. Figure 2 shows a schematic of the incremental and load correcting nonlinear solution strategies. Obviously, the load correction procedure is more accurate than the incremental procedure.

The matrices and vectors of Eq. 5(b) are obtained by applying standard coordinate transformation techniques to the element level equations. Direct stiffness assembly of the elemental matrices leads to the structure matrices of Eq. 5(b).

Beam Element Matrices - The elemental mass, [m], and geometric stiffness, $[k_G]$, matrices are obtained using finite element approximations

$$[m] = \int_o^{\ell} \bar{m}\,[N]^T\,[N]\,dx \quad (6a)$$

$$[k_G] = F \int_o^{\ell} (\{N_a'\}\{N_a'\}^T + \{N_f'\}\{N_f'\}^T)dx \quad (6b)$$

where

$$[N] = \begin{bmatrix} N_1 & 0 & 0 & N_4 & 0 & 0 \\ 0 & N_2 & N_3 & 0 & N_5 & N_6 \end{bmatrix}$$

$$\{N_a'\}^T = [0 \quad dN_1/dx \quad 0 \quad 0 \quad dN_4/dx \quad 0]$$

$$\{N_f'\}^T = [0 \quad dN_2/dx \quad dN_3/dx \quad 0 \quad dN_5/dx \quad dN_6/dx]$$

N_i (i=1,2,...6) are the beam element shape functions defined in Fig. 3,

subscripts a, f signify axial and flexure, respectively, $\bar{m}$ is the mass per unit length, ℓ is the beam element length, F is the element axial force (tension postive) and superscript T is used to signify transpose. The matrices in Eqs. 6(a) and (b) can be integrated exactly and are given in several standard structural analysis texts, e.g., Przemieniecki (Ref. 6).

Unfortunately, the finite element procedure does not adequately represent the elastic element stiffness matrix in the post-local-buckling range. However, an exact static elastic stiffness matrix and equivalent nodal force vector can be constructed using the principal of virtual forces and the flexibility-stiffness transformation technique as outlined by McGuire and Gallagher (Ref. 5). The internal forces required in the principle of virtual forces are given by the equations of static equilibrium. Since the equilibrium equations are independent of the cross sectional properties for the beam of Fig. 4, an exact flexibility matrix, [f], is

$$[f] = \int_0^{\ell} [Q]^T [C]^{-1} [Q] \, dx \tag{7}$$

where

$$[Q] = \begin{bmatrix} -1 & 0 & 0 \\ 0 & \xi - 1 & \xi \end{bmatrix}$$

- matrix of shape functions for the internal force distribution,

$$[C]^{-1} = \begin{bmatrix} \frac{1}{EA(x)} & 0 \\ 0 & \frac{1}{EI(x)} \end{bmatrix}$$

and the other symbols are as previously defined.

The flexibility matrix of Eq. 7 is evaluated using a 15 point composite Simpson rule. Quadrature is required in the evaluation of Eq. 7 due to the

arbitrary variation of A(x) and I(x) in the post-local-buckling range. The area and moment of inertia are calculated exactly at each of the quadrature points.

After obtaining the flexibility matrix, the element elastic stiffness matrix, $[k_E]$, can be calculated from (Ref. 5)

$$[k_E] = \begin{bmatrix} [f]^{-1} & [f]^{-1}[\Phi]^T \\ [\Phi][f]^{-1} & [\Phi][f]^{-1}[\Phi]^T \end{bmatrix} \tag{8}$$

where $[\Phi]$ is the element equilibrium matrix. The equilibrium matrix is constructed by relating the flexibility forces, $\{F^f\}$, to the support forces, $\{F^s\}$, of Fig. 4, i.e.,

$$\{F^s] = [\Phi]\{F^f\}$$

or

$$\begin{Bmatrix} F_1^s \\ F_2^s \\ F_3^s \end{Bmatrix} = \begin{bmatrix} -1 & 0 & 0 \\ 0 & 1/\ell & 1/\ell \\ 0 & -1/\ell & -1/\ell \end{bmatrix} \begin{Bmatrix} F_1^f \\ F_2^f \\ F_3^f \end{Bmatrix} \tag{9}$$

Substituting the flexibility and equilibrium matrices into Eq. 8 results in an exact element elastic stiffness matrix for the beam element in the post-local-buckling range.

The flexibility approach can also be usd to construct the exact element fixed-end forces. First calculate the displacements, $\{v^f\} = [v_1\ v_3\ v_6]^T$, in terms of the applied internal bending moment, M(x), via

$$\{v^f\} = \int_0^{\ell} [Q]^T [C]^{-1} \{p\}\, dx \tag{10}$$

where $\{p\} = [0\ M(x)]^T$. Due to the variation of A(x) and I(x) in $[C]^{-1}$ of Eq. 10, a 15 point composite Simpson rule is utilized for the integration.

The fixed-end forces corresponding to the flexibility degrees of freedom,

$$\{F_F^f\} = - [f]^{-1} \{v^f\} \tag{11}$$

The fixed-end forces at the support degrees of freedom, $\{F_F^s\}$, as obtained

from equilibrium are

$$\{F_F^S\} = [\Phi]\ \{F_F^f\} + \{\Phi_q\} \tag{12}$$

where

$$\{\Phi_q\} = q\ell/2\ [0\ 1\ 1]^T$$

- uniform distributed load contribution to equilibrium; and

q - uniform distributed load per unit length.

The fixed-end forces of Eqs. 11 and 12 are assembed into the structure load vector $\{P(t+\Delta t)\}$ of Eq. 5(b) once they have been transformed into the global coordinate system.

Load Correcting Wilson-θ Formulation - The Wilson-θ method for integrating the dynamic equilibrium equations of Eq. 5(b) is essentially an extension of the linear acceleration method (linear variation of acceleration from time t to time $t + \Delta t$ is assumed, Δt is the time increment). The Wilson-θ method assumes that the acceleration varies linearly from time t to time $t + \theta\Delta t$ where $\theta \geq 1$ (Ref. 1). For $\theta = 1.0$, the Wilson-θ method reduces to the linear acceleration scheme, but for unconditional stability, it is necessary to use $\theta \geq 1.37$ and usually a value of $\theta = 1.40$ is chosen.

The solution of the nonlinear dynamic equilibrium equations (Eq. 5(b)) using the load correcting Wilson-θ method can be summarized as:

1. Initialization

   (a) Set the initial values for the displacements $\{v(0)\}$, the velocities $\{\dot{v}(0)\}$ and the forces $\{P(0)\}$. Zero initial displacements and velocities are assumed in this paper.

   (b) Calculate the initial accelerations $\{\ddot{v}(0)\}$:

   $$[M]\ \{\ddot{v}(0)\} = \{P(0)\}$$

   (c) Select a time step Δt, the factor θ (usually 1.4) and calculate

the time integration constants:

$$\tau = \theta\Delta t;\ a_1 = 3/\tau\ ;\ a_2 = 2a_1;\ a_3 = \tau/2;\ a_4 = 6/\tau^2$$

2. (a) Calculate the effective stiffness matrix $[\overline{K}(t_i)]$:

$$[\overline{K}(t_i)] = [K_E(t_i)] + [K_G(t_i)] + a_4[M]$$

(b) Calculate the extended incremental load $\{\hat{dP}_{i+1}\}$ for the time interval t_i to $t_i + \tau$ using linear interpolation:

$$\{\hat{dP}_{i+1}\} = \theta(\{P_{i+1}\} - \{P_i\})$$

(c) Calculate the internal balanced force vector $\{F_E(t_i)\}$:

$$\{F_E(t_i)\} = \{F_E(t_{i-1})\} + ([K_E(t_i)] + [K_G(t_i)]\{dv_i\}$$

$$\{F_E(0)\} \equiv \{0\}$$

(d) Calculate the effective load vector $\{\overline{P}_{i+1}\}$ at time $t_i + \tau$:

$$\{\overline{P}_{i+1}\} = \{P_i\} + \{dP_{i+1}\} + [M](a_2\{\dot{v}_i\} + 2\{\ddot{v}_i\}) - \{F_E(t_i)\}$$

(e) Solve for the extended incremental displacements $\{\hat{dv}_{i+1}\}$ for time increment τ:

$$[\overline{K}(t_i)]\{\hat{dv}_{i+1}\} = \{\overline{P}_{i+1}\}$$

(f) Calculate the extended incremental accelerations $\{\hat{d\ddot{v}}_{i+1}\}$ for time increment τ:

$$\{\hat{d\ddot{v}}_{i+1}\} = a_4[\hat{dv}_{i+1}\} - a_2\{\dot{v}_i\} - 3\{\ddot{v}_i\}$$

(g) Calculate the incremental accelerations $\{d\ddot{v}_{i+1}\}$ for the time interval Δt:

$$\{d\ddot{v}_{i+1}\} = (1/\theta)\{\hat{d\ddot{v}}_{i+1}\}$$

(h) Calculate the incremental velocities $\{d\dot{v}_{i+1}\}$ and displacements $\{dv_{i+1}\}$ for the time interval Δt:

$$\{d\dot{v}_{i+1}\} = \Delta t\{\ddot{v}_i\} + (\Delta t/2)\{d\ddot{v}_{i+1}\}$$

$$\{dv_{i+1}\} = \Delta t\{\dot{v}_i\} + (\Delta t^2/2)\{\ddot{v}_i\} + (\Delta t^2/6)\{d\ddot{v}_{i+1}\}$$

(i) Accumulate the displacement, velocity and acceleration vectors at

time $t_{i+1} = t_i + \Delta t$:

$$\{v_{i+1}\} = \{v_i\} + \{dv_{i+1}\}$$

$$\{\dot{v}_{i+1}\} = \{\dot{v}_i\} + \{d\dot{v}_{i+1}\}$$

$$\{\ddot{v}_{i+1}\} = \{\ddot{v}_i\} + \{d\ddot{v}_{i+1}\}$$

(j) Accumulate the static member end forces at time $t_{i+1} = t_i + \Delta t$:

$$\{f_s(t_{i+1})\} = \{f_s(t_i)\} + ([k_E(t_i) + [k_G(t_i)]]\{dv_{i+1}\}$$

(k) Output the results.

The above algorithm shows that an efficient assembly and solution strategy is required for solving nonlinear dynamic problems. Consequently, the assembly and symmetric Gauss-Crout profile (or skyline) solution algorithm of Taylor (Ref. 7) was utilized in the present investigation.

NUMERICAL RESULTS

The developed computer program follows the outlined analytical procedure and can be used for either dynamic or static loading as well as for linear or nonlinear analysis. The nonlinear problems due to local buckling and geometric changes are solved using either an incremental or load correcting strategy (Fig. 2). The unbraced frame geometry and loading condition shown in Fig. 5 was used for both static and dynamic analyses. The dimensions for the rectangular tubular section used are shown Fig. 5(c). All analyses were performed on the IBM 370/165 computer available at the University of Kentucky.

Static Analysis - A static analysis was carried out on the unbraced frame shown in Fig. 5 to verify the post-local-buckling portion of the dynamic analysis program. For a static analysis, the time integration constants are zero and $\Delta t, \theta$ are both set equal to one. The dynamic program uses either an incremental tangent stiffness procedure or a load correcting strategy to

incorporate the nonlinear behavior into the analysis. For the results presented in this paper, twenty load steps were used for each analysis.

The unbraced frame of Fig. 5 was analyzed earlier by Wang and Blandford (Ref. 11) using a step iterative secant stiffness procedure and a post-local-buckling behavior based on the moment-curvature table which neglected the axial stress contributions to the post-local-buckling behavior. In this paper, both the bending and axial force effects on the post-local-buckling behavior are included in the formulation. For the given loading condition, the bending moments at the ends of several members are shown in Table 1 with the moment numbers being defined in Fig. 5(b). The linear elastic frame results are shown in column 2 of Table 1 for the purpose of comparison. The calculated moments in the post-local buckling range of Ref. 11 are shown in column 3. The incremental and load correcting results of this paper are presented in columns 4 and 5, respectively. The moments obtained from these two methods are very close. The differences between the results in columns 3 and 4 or 5 are mainly due to the effects of axial stress on local buckling which were not accounted for in the earlier study. For the problem considered, only a slight moment redistribution is experienced due to local buckling as compared to the results for an elastic prismatic frame.

Table 2 presents moment results for the linear elastic, locally buckled, geometric nonlinear and combined local buckling and geometric nonlinearity analyses. The nonlinear analyses of Table 2 are based on using 20 load steps, the load correcting solution strategy and the unbraced frame of Fig. 5. Table 2 shows that the effects of geometric change (beam-column and P-delta effects) on the calculated moments (column 4) are more severe than the moment redistribution caused by local buckling (column 3). Furthermore, Table 2 shows that the combined nonlinear influences (column 5) results in a tremendous moment redistribution at several beam to column connections. For

example, moment number 9 increases by over 20 percent whereas moment number 1 decreases by over 85 percent when compared with the linear elastic results.

Dyanmic Analysis - The unbraced frame of Fig. 5 was also analyzed subjected to the time dependent uniform load q and horizontal loads H as shown in Fig. 6. A time increment of $t = 0.04$ seconds and $\theta = 1.40$ were used in the dynamic analysis. The top floor horizontal displacement versus time response curves are shown in Fig. 6. The duration of the triangle shaped concentrated force H is about twice the natural period of the structure under consideration.

In the figure, the curve for the linear elastic case shows a plateau from 1.20 to 2.20 seconds while the curve considering the local buckling behavior reaches the plateau at about the same time but rises to a sharp peak in the late portion of the plateau. The maximum magnitude of the drift for the case considering local buckling is 20 percent larger than that corresponding to the linear elastic case. The dramatic jump in the curve is a result of the combined action of the constant uniform load q and the linearly varied force H. Note that the jump happens after the maximum value of H has been reached.

The peak value of geometric nonlinear response is about 38 percent larger than that of linear elastic response. However, the free vibration portion of the curve is very weak. This could be due to poor geometric nonlinear modeling once the sidesway force is zero. When the sidesway force is removed the beam-column effect dominates and generally two column finite elements are required to adequately approximate the dominant beam-column behavior. The maximum magnitude of the drift is 54 percent larger when both local buckling and geometric nonlinearity are included.

SUMMARY AND CONCLUSIONS

Both static and dynamic results for plane frame structures in the post-local-buckling range which include first-order geometric nonlinearity have been presented. The post-local-buckling behavior was included using the effective width concept. Both axial and bending stresses were utilized in calculating the effective width. An exact elastic stiffness, finite element geometric stiffness and consistent mass were used to discretize the nonlinear dynamic equilibrium equations. The solution of the nonlinear dynamic equations was obtained using a load correction strategy coupled with the implicit Wilson-θ time integration scheme. It was found that the solution scheme is accurate and that the method is well suited for the type of problems considered.

Both the static and dynamic results showed stress redistribution in the post-local-buckling range. However, for the problems considered, the stress redistribution caused by the beam-column and P-delta effects was more significant than the stress redistribution caused by local buckling. Furthermore, including both local buckling and geometric nonlinearity resulted in the lagest percentage stress redistribution as compared with the linear elastic results. These results clearly demonstrate the need for including beam-column and P-delta effects in the frame analysis of light gage steel structures.

Table 1

Comparison of Locally-Buckled Unbraced Frame Moments for the Static Case

(H = 60 lb, q = 2.4 lb/in)

Moment Number (1)	Moment of Elastic Prismatic Frame in-lbs (2)	Moment of Locally Buckled Frame in in-lbs: Wang and Blandford (3)	Incremental Analysis (4)	Load Correcting Analysis (5)
1	172.32	156.10	168.24	168.45
2	-3226.50	-3201.70	-3193.50	-3191.20
5	- 536.40	- 551.50	- 539.02	- 539.22
6	-3965.10	-3896.30	-3904.90	-3901.00
9	1972.40	2016.20	2002.80	2006.40
10	933.58	957.70	942.72	944.59
11	- 397.18	- 406.30	- 403.70	- 405.37
12	- 172.32	- 156.10	- 168.24	- 168.45

Table 2

Comparison of Nonlinear Unbraced Frame Moments for the Static Case

(H = 60 lb, q = 2.4 lb/in)

Moment Number (1)	Moment of Elastic Prismatic Frame in-lbs (2)	Moment of Nonlinear Frame in in-lbs: Local Buckling (3)	Geometric Nonlinear (4)	Local Buckling & Geometric Nonlinear (5)
1	172.32	168.45	40.14	23.36
2	-3226.50	-3191.20	-3339.50	-3312.10
5	- 536.40	- 539.22	- 864.13	- 899.79
6	-3965.10	-3901.00	-4238.10	-4189.30
9	1972.40	2006.40	2340.90	2410.80
10	933.58	944.59	1199.90	1242.90
11	- 397.18	- 405.37	- 335.73	- 343.14
12	- 172.32	- 168.45	- 40.14	- 23.26

APPENDIX I - REFERENCES

1. Bathe, K.J. and Wilson, E.L., "Stability and Accuracy Analysis of Direct Integration Methods," Earthquake Engrg. Struct. Dynamics, Vol. 1, pp. 283-291, 1973.

2. Blandford, G.E., Wang, S.T. and Wang, N.T., "Dynamic Behavior of Locally Buckled Frames," Proceedings of the Sixth International Specialty Conference on Cold-Formed Steel Structures, St. Louis, MO, 1982.

3. Culver, C.G. and Tassel, R.A., "Shock Loading of Thin Compression Elements," Proceedings of the First Specialty Conference on Cold-Formed Structures, University of Missouri-Rolla, MO, 1971.

4. Johnson, A.L. and Winter, G., "Behavior of Stainless Steel Columns and Beams," J. Struct. Div., ASCE, Vol. 92, No. ST5, pp. 97-118, 1968.

5. McGuire, W. and Gallagher, R.H., Matrix Structural Analysis, John Wiley & Sons, New York, Chapters 4 and 9, 1979.

6. Przemieniecki, J.S., Theory of Matrix Structural Analysis, McGraw-Hill, New York, Chapters 11 and 15, 1968.

7. Taylor, R.L. in O.C. Zienkiewicz, The Finite Element Method, Third Edition, McGraw-Hill, New York, Chapter 24, 1977.

8. Vaidya, N.R. and Culver, C.G., "Impact Loading of Thin-Walled Columns," Proceedings of the First Specialty Conference on Cold-Formed Steel Structures, University of Missouri-Rolla, MO, 1971.

9. Wang, S.T. and Winter, G., "Cold Rolled Austenitic Stainless Steel Material Properties and Structural Performance," Report 334, Department of Structural Engineering, Cornell University, Ithaca, New York, 1969.

10. Wang, S.T., Errera, S.J. and Winter, G., "Behavior of Cold-Rolled Stainless Steel Members, J. Struct. Div., ASCE, Vol. 101, No. ST11, pp. 2337-2357, 1975.

11. Wang, S.T. and Blandford, G.E., "Stability Analysis of Locally Buckled Frames," Proceedings of the Fourth International Specialty Conference on Cold-Formed Steel Structures, St. Louis, MO, 1978.

12. Wilson, E.L., Farhoomad, I. and Bathe, K.J., "Nonlinear Dynamic Analysis of Complex Structures," Earthquake Engrg. Struct. Dynamics, Vol. 1, pp. 241-252, 1973.

13. Zaroni, E.A. and Culver, C.G., "Impact Loading of Thin-Walled Beams," Proceedings of the First Specialty Conference on Cold-Formed Steel Structures, University of Missour-Rolla, MO, 1971.

APPENDIX II - NOTATION

a_1, a_2, a_3, a_4 - time integration constants

b - effective width of compression plate element

d - symbol used to signify increment

i - time step number

$\overline{m}$ - mass density per unit length

q - magnitude of uniform load

t - plate thickness, or time

Δt - time increment

w - flat width of the compression plate element exclusive of fillets

A - cross sectional area

E - modulus of elasticity

$(EA)_{eff}$ - effective axial rigidity

$(EI)_{eff}$ - effective flexural rigidity

F - beam element axial force (tension positive)

I - moment of inertia

K - buckling coefficient

ℓ - beam element length

ξ - effective width equation modification factor, or nondimensionalized interpolation coordinate

σ_{cr} - critical local buckling stress

σ_{max} - maximum edge stress

θ - time weighting coefficient used in the Wilson-θ method

τ - extended time increment

$\{f_s(t)\}$ - static member end forces at time t

$\{p\}$ - internal force vector

$\{F^f\}$ - beam element flexibility formulation force vector

$\{F_F^f\}$ - beam element fixed-end forces at the flexibility force degrees of freedom

$\{F^s\}$ - beam element support reaction vector in the flexibility formulation

$\{F_F^s\}$ - beam element fixed-end forces at the flexibility support degrees of freedom

$\{F_E(t)\}$ - structure elastic force vector at time t

$\{F_I(t)\}$ - structure inertia force vector at time t

$\{N_a'\}$ - derivative beam element shape function vector for evaluating the axial deformation dependent geometric stiffness

$\{N_f'\}$ - derivative beam element shape function vector for evaluating the bending deformation dependent geometric stiffness

$\{P(t)\}$ - structure external load vector at time t

$\{\overline{P}_{i+1}\}$ - effective structure load vector at time $t_i + \tau$

$\{dF_E\}$ - incremental structure elastic force vector

$\{dF_I\}$ - incremental structure inertia force vector

$\{\hat{dP}_{i+1}\}$ - extended incremental structure load vector

$\{v^f\}$ - beam element displacement vector at the flexibility force degrees of freedom

$\{v_i\}$ - displacement vector at time t_i

$\{\dot{v}_i\}$ - velocity vector at time t_i

$\{\ddot{v}_i\}$ - acceleration vector at time t_i

$\{dv_{i+1}\}$ - incremental displacement vector

$\{d\dot{v}_{i+1}\}$ - incremental velocity vector

$\{d\ddot{v}_{i+1}\}$ - incremental acceleration vector

$\{\hat{dv}_{i+1}\}$ - extended incremental displacement vector

$\{\hat{d\ddot{v}}_{i+1}\}$ - extended incremental acceleration vector

$\{\Phi_q\}$ - uniform distributed load equilibrium vector

$[C]^{-1}$ - matrix inverse of the beam element constitutive matrix

$[f]$ - beam element flexibility matrix

$[k_E]$ - beam element elastic stiffness matrix

$[k_G]$ - beam element geometric stiffness matrix

$[K_E(t)]$ - structure tangent elastic stiffness matrix at time t

$[K_G(t)]$ - structure tangent geometric stiffness matrix at timet

$[\overline{K}(t)]$ - effective nonlinear stiffness matrix at time t

$[m]$ - beam element consistent mass matrix

$[M]$ - structure mass matrix

$[N]$ - matrix of beam element shape functions

$[Q]$ - matrix of beam element internal force shape functions

$[\Phi]$ - beam element equilibrium matrix

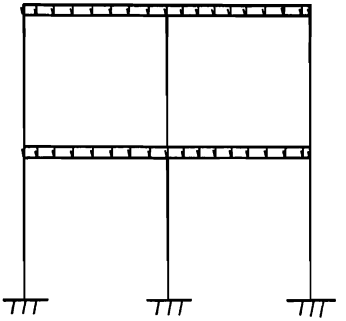

(a) Rigid Plane Frame

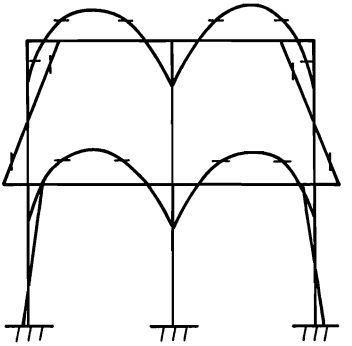

(b) Moment Distribution

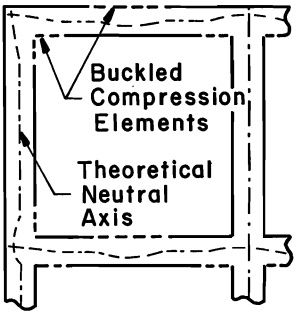

(c) Buckled Members and Neutral Axis Shift

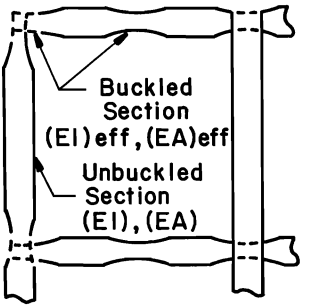

(d) Variation of Equivalent Effective Flexural and Axial Rigidities

FIG. 1 - RIGID PLANE FRAME IN THE POST-LOCAL-BUCKLING RANGE

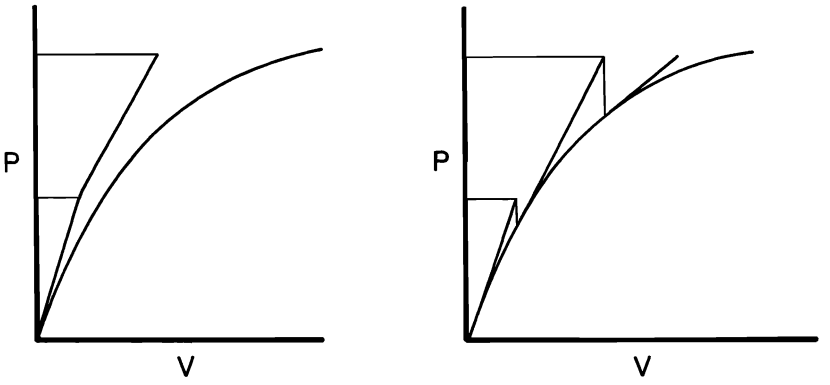

(a) Incremental Scheme (b) Load Correction Scheme

FIG. 2 - NONLINEAR SOLUTION STRATEGY SCHEMATICS

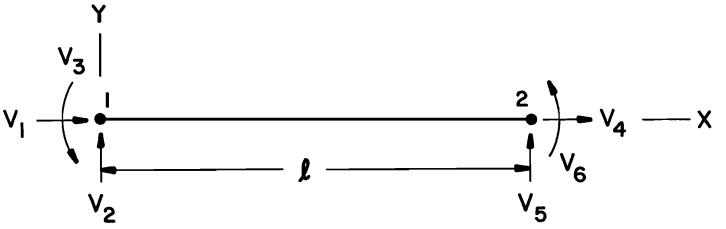

(a) Beam Element Displacements

$$N_1 = 1 - \xi \quad ; \quad N_4 = \xi$$

$$N_2 = 1 - 3\xi^2 + 2\xi^3 \quad ; \quad N_5 = 3\xi^2 - 2\xi^3$$

$$N_3 = x(1 - 2\xi + \xi^2) \quad ; \quad N_6 = x(\xi - \xi^2)$$

(b) Beam Element Shape Functions ($\xi = x/\ell$)

FIG. 3 - BEAM FINITE ELEMENT

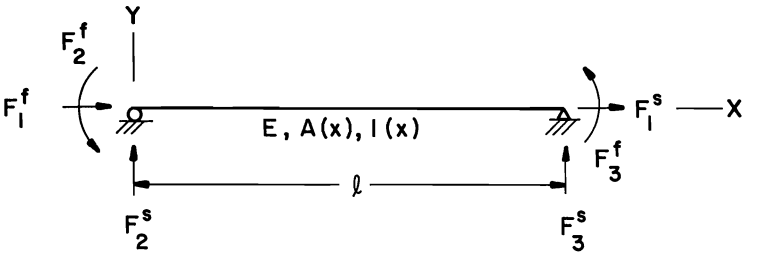

FIG. 4 - BEAM FLEXIBILITY ELEMENT

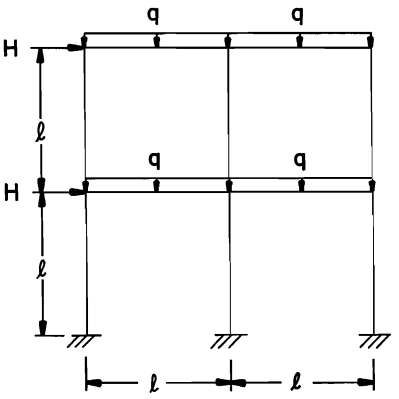

(a) Unbraced Frame

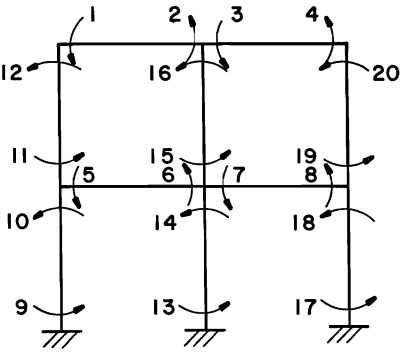

(b) Member End Moment Numbers

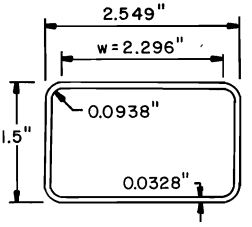

(c) Dimensions for Rectangular Tubular Section

FIG. 5 - UNBRACED FRAME GEOMETRY AND LOADING
(ℓ = 100", 1 in = 25.4 mm)

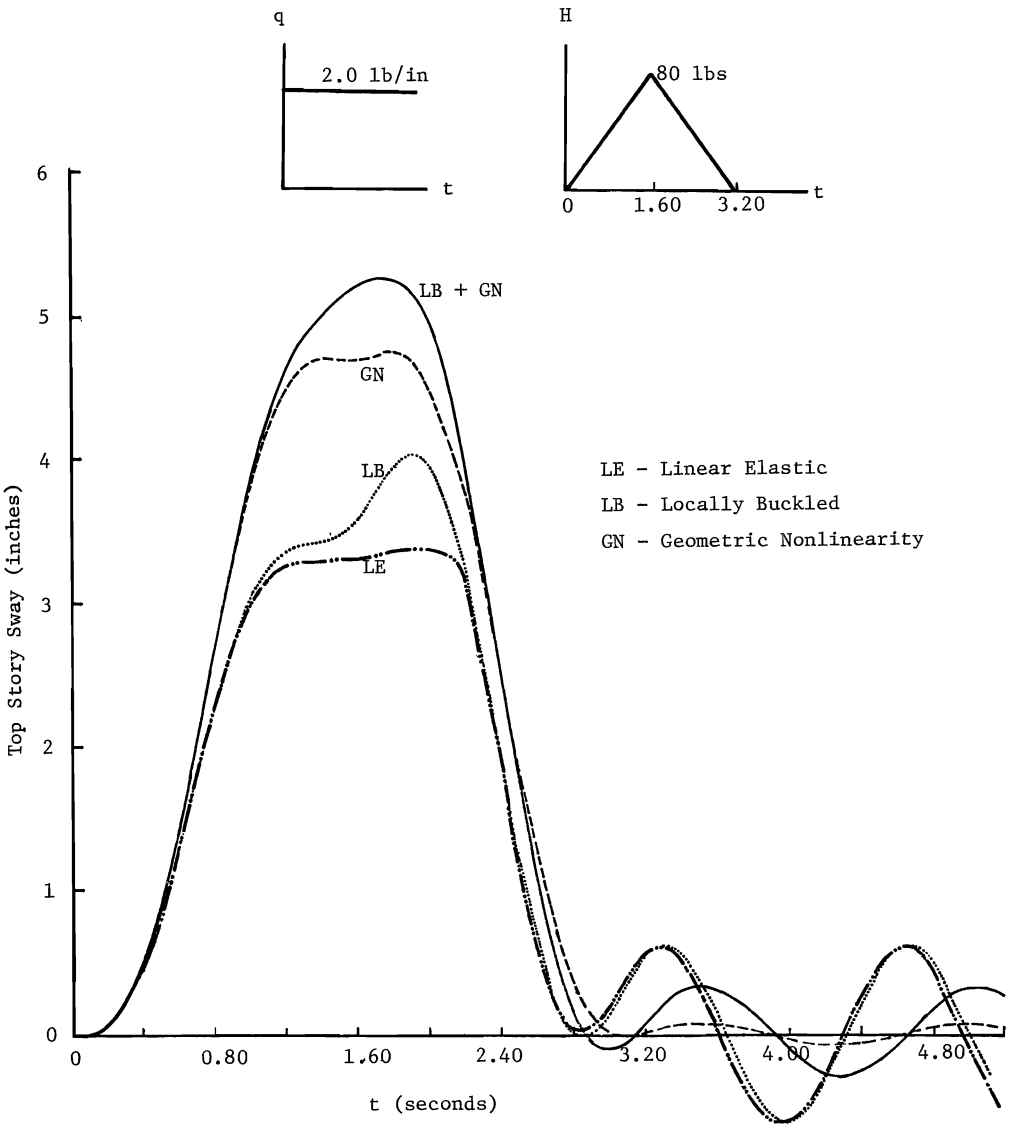

FIG. 6 - SWAY - TIME VARIATION FOR THE UNBRACED FRAME
(1 lb/in = 175 N/m, 1 lb = 4.45 N, 1 in = 25.4 mm)